

# Toroid Morphology by ABC-Type Amphiphilic Rod–Coil Molecules at the Air–Water Interface

Libin Liu,<sup>†</sup> Jung-Keun Kim,<sup>†</sup> Ray Gunawidjaja,<sup>‡</sup> Vladimir V. Tsukruk,<sup>\*,‡</sup> and Myongsoo Lee<sup>\*,†</sup>

Center for Supramolecular Nano-Assembly, Department of Chemistry, Yonsei University, Seoul 120-749, Korea, and School of Materials Science and Engineering, Georgia Institute of Technology, Atlanta, Georgia 30332

Received May 4, 2008. Revised Manuscript Received September 2, 2008

The interfacial and aggregation behavior of the ABC-type amphiphilic molecules with semirigid dumbbell-shaped core and variable length of hydrophobic branched tails ( $R=(CH_2)_nCH_3$  with  $n = 5$  (**1**), 9 (**2**), 13 (**3**)) were investigated. At low surface pressure, smooth, uniform monolayers were formed at the air–water interface by molecules **1** and **2**, whereas for molecule **3** unique 2D toroid aggregates have been formed. These aggregates were relatively stable within a range of surface pressure and spreading solution concentration. Upon compression, the 2D toroid aggregates collapsed into large, round 3D aggregates. Finally, the choice of spreading solvent has a great influence on aggregation formation into 2D or 3D micelles as a result of the variable balance of the hydrophobic interactions of branched tails and the  $\pi$ – $\pi$  stacking interaction between aromatic segments.

## Introduction

Recent studies on novel functional materials have received a great deal of attention because of their potential in the construction of elaborately defined supramolecular nanostructures.<sup>1</sup> Rod–coil molecules consisting of a rigid rod and a flexible coil block are excellent candidates for creating well-defined supramolecular structures via a process of spontaneous organization.<sup>2</sup> In contrast to coil–coil block molecules, rod–coil molecules can form well-ordered macrostructures in spite of their low molecular weight because the anisometric molecular shape and stiff rodlike conformation of the rod segment impart orientational organization. A variety of nanostructures, such as 2D, zigzag, ribbonlike, helical, and cylindrical structures have been observed for rod–coil molecules by different research groups.<sup>3–7</sup> By way of contrast, the investigation of the behavior of rod–coil molecules at the air–water interface has been reported only a few times in the literature.<sup>8,9</sup> The air–water interface provides an ideal environment for fabricating surface aggregates from amphiphilic block copolymers, given the precise control of various experimental

conditions including the continuous variation of the surface density.

The Langmuir–Blodgett (LB) technique allows the fabrication of monomolecular and ultrathin films through the deposition of monolayers from the air–water interface to solid substrates.<sup>10</sup> Indeed, LB films typically exhibit a high degree of molecular order that is induced at the water surface by 2D geometrical restriction and compressive stresses.<sup>11</sup> Studies on LB monolayers of amphiphilic block copolymers revealed 2D surface aggregates that range from small circular objects to cylindrical structures and to large planar aggregates.<sup>12–14</sup> For amphiphilic rod–coil molecules, the rigid-rod segments have been employed as a structural element in the construction of various shape-persistent molecular architectures<sup>15</sup> and liquid-crystalline materials.<sup>16</sup> The extended  $\pi$ -conjugated electronic structure that these compounds offer raises considerable interest in the potential wirelike properties of these molecules when used to bridge molecular

\* To whom correspondence should be addressed. E-mail: vladimir@mse.gatech.edu and mslee@yonsei.ac.kr.

<sup>†</sup> Yonsei University.

<sup>‡</sup> Georgia Institute of Technology.

(1) (a) Lehn, J.-M. *Proc. Natl. Acad. Sci. U.S.A.* **2002**, *99*, 4763. (b) Förster, S.; Plantenberg, T. *Angew. Chem., Int. Ed.* **2002**, *41*, 688. (c) Hoeben, F. J. M.; Jonkheijm, P.; Meijer, E. W.; Schenning, A. P. H. *J. Chem. Rev.* **2005**, *105*, 1491. (d) Cornelissen, J. J. L.; Rowan, M. A. E.; Nolte, R. J. M.; Sommerdijk, N. A. J. M. *Chem. Rev.* **2001**, *101*, 4039. (e) Ajayaghosh, A.; Varghese, R.; George, S. J.; Vijayakumar, C. *Angew. Chem., Int. Ed.* **2006**, *45*, 1141.

(2) (a) Lee, M.; Cho, B.-K.; Zin, W.-C. *Chem. Rev.* **2001**, *101*, 3869. (b) Lee, M.; Yoo, Y.-S. *J. Mater. Chem.* **2002**, *12*, 2161.

(3) (a) Chen, J. T.; Thomas, E. L.; Ober, C. K.; Mao, G.-P. *Science* **1996**, *273*, 343. (b) Chen, J. T.; Thomas, E. L.; Ober, C. K.; Hwang, S. S. *Macromolecules* **1995**, *28*, 1688. (c) Gopalan, P.; Zhang, Y.; Li, X.; Wiesner, U.; Ober, C. K. *Macromolecules* **2003**, *36*, 3357.

(4) (a) Park, J.-W.; Thomas, E. L. *Macromolecules* **2004**, *37*, 3532. (b) Park, J.-W.; Thomas, E. L. *Adv. Mater.* **2003**, *15*, 585. (c) Park, J.-W.; Thomas, E. L. *J. Am. Chem. Soc.* **2002**, *124*, 514.

(5) (a) Zubarev, E. R.; Pralle, M. U.; Sone, E. D.; Stupp, S. I. *Adv. Mater.* **2002**, *14*, 198. (b) Sayar, M.; Stupp, S. I. *Macromolecules* **2001**, *34*, 7135. (c) Sayar, M.; Solis, F. J.; Olvera de la Cruz, M.; Stupp, S. I. *Macromolecules* **2000**, *33*, 7226.

(6) (a) Oh, N.-K.; Zin, W.-C.; Im, J.-H.; Ryu, J.-H.; Lee, M. *Chem. Commun.* **2004**, *9*, 1092. (b) Ryu, J.-H.; Oh, N.-K.; Zin, W.-C.; Lee, M. *J. Am. Chem. Soc.* **2004**, *126*, 3551.

(7) (a) Percec, V.; Glodde, M.; Bera, T. K.; Miura, Y.; Shiyonovskaya, I.; Singer, K. D.; Balagurusamy, V. S. K.; Heiney, P. A.; Schnells, I.; Rapp, A.; Spiess, H.-W.; Hudson, S. D.; Duan, H. *Nature* **2002**, *419*, 384. (b) Zeng, X.; Ungar, G.; Liu, Y.; Percec, V.; Dulcey, A. E.; Hobbs, J. K. *Nature* **2004**, *428*, 157. (c) Percec, V.; Dulcey, A. E.; Balagurusamy, V. S. K.; Miura, Y.; Smidrkal, J.; Peterca, M.; Nummelin, S.; Edlund, U.; Hudson, S. D.; Heiney, P. A.; Duan, H.; Magonov, S. N.; Vinogradov, S. A. *Nature* **2004**, *430*, 764. (d) Ungar, G.; Liu, Y.; Zeng, X.; Percec, V.; Cho, W.-D. *Science* **2003**, *299*, 1208.

(8) (a) Li, H. B.; Liu, Q. T.; Xu, M.; Bu, W. F.; Lin, X. K.; Wu, L. X.; Shen, J. C. *J. Phys. Chem. B* **2005**, *109*, 2855. (b) Zhang, J.; Cao, H. Q.; Wan, X. H.; Zhou, Q. F. *Langmuir* **2006**, *22*, 6587.

(9) (a) Tsukruk, V. V.; Genson, K.; Peleshanko, S.; Markutsya, S.; Lee, M.; Yoo, Y.-S. *Langmuir* **2003**, *19*, 495. (b) Holzmueller, J.; Genson, K. L.; Park, Y.; Yoo, Y.-S.; Park, M.-H.; Lee, M.; Tsukruk, V. V. *Langmuir* **2005**, *21*, 6392. (c) Liu, L.; Moon, K.-S.; Gunawidjaja, R.; Lee, E.; Tsukruk, V. V.; Lee, M. *Langmuir* **2008**, *24*, 3930.

(10) Ulman, A. *An Introduction to Ultrathin Organic Films: From Langmuir-Blodgett to Self-Assembly*; Academic Press: Boston, MA, 1991.

(11) Möhwald, H. *Rep. Prog. Phys.* **1993**, *56*, 653.

(12) (a) Zhu, J.; Eisenberg, A.; Lennox, R. B. *J. Am. Chem. Soc.* **1991**, *113*, 5583. (b) Zhu, J.; Lennox, R. B.; Eisenberg, A. *Langmuir* **1991**, *7*, 11579. (c) Zhu, J.; Eisenberg, A.; Lennox, R. B. *Makromol. Chem.* **1992**, *53*, 211. (d) Zhu, J.; Lennox, R. B.; Eisenberg, A. *J. Phys. Chem.* **1992**, *96*, 4727. (e) Zhu, J.; Eisenberg, A.; Lennox, R. B. *Macromolecules* **1992**, *25*, 6547. (f) Zhu, J.; Eisenberg, A.; Lennox, R. B. *Macromolecules* **1992**, *25*, 6556.

(13) (a) Gonçualves da Silva, A. M.; Filipe, E. J. M.; d'Oliveira, J. M. R.; Martinho, J. M. G. *Langmuir* **1996**, *12*, 6547. (b) Gonçualves da Silva, A. M.; Simoes Gamboa, A. L.; Martinho, J. M. G. *Langmuir* **1998**, *14*, 5327.

(14) Cox, J. K.; Yu, K.; Constantue, B.; Eisenberg, A.; Lennox, R. B. *Langmuir* **1999**, *15*, 7714.

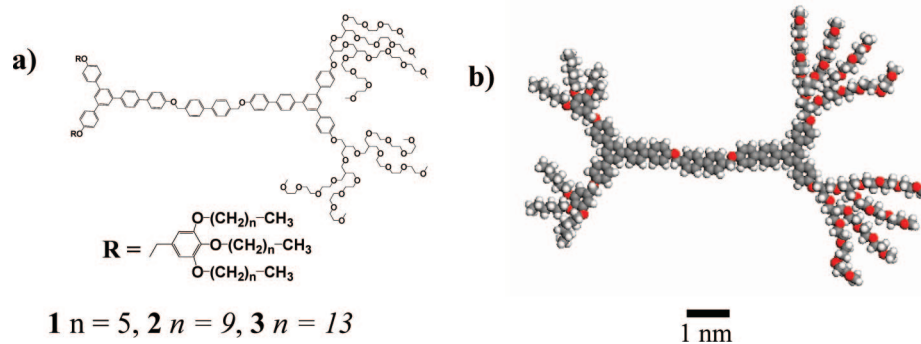


**Figure 1.** (a) Chemical structure of ABC-type molecules with variable hydrophobic tail lengths and (b) the corresponding representative molecular model, **1**.

photoactive centers<sup>17</sup> or to span a nanoscopic gap between macroscopic electrodes.<sup>18,19</sup> Correspondingly, water-soluble flexible chains (e.g., PEO) can be submerged in the water subphase during compression, thus forming a thin polymer layer enriched with water molecules beneath the hydrophobic rod blocks. Changing the effective composition at the air–water interface upon compression for these rod–coil molecules is expected to generate highly ordered films with defined thickness and controlled architecture, as reported in linear and star block copolymers.<sup>9,20</sup>

In our previous work, we investigated the aggregation behavior of ABC-type amphiphilic molecules with a semirigid dumbbell-shaped core and variable hydrophobic lengths in a selective solvent (Figure 1). In solution, these molecules formed stable 3D micelles predominantly adopting mixed spherical and short cylindrical, toroidal, and long cylindrical morphologies for  $n = 5$  (**1**), 9 (**2**), and 13 (**3**), respectively.<sup>21</sup> Overall, they exhibit the usual systematic transformation from highly curved to a more flat interface with increasing hydrophobic component content.

Herein, we further investigated the aggregation behavior of these semirigid dumbbell-shaped low-molecular-weight molecules within Langmuir monolayers at the air–water interface and within LB monolayers on silicon substrates in comparison with those formed in solution and demonstrate how the fabrication approaches control the molecular aggregation.

## Experimental Section

**Materials.** The rod–coil molecules, which consist of a rod segment with terminal hydrophilic polyether dendrons at one end and hydrophobic branches at the other end, used in this study are depicted in Figure 1. Their syntheses have been reported elsewhere.<sup>21</sup>

**Monolayer Fabrication.** Langmuir isotherms at the air–water interface and LB deposition onto a silicon substrate were conducted at room temperature using a KSV 2000 LB minitrough according

to the usual procedure.<sup>22</sup> A 40–120  $\mu\text{L}$  volume of dilute polymer solution at concentrations of 0.2 and 0.5 mg/mL in chloroform (HPLC grade) was deposited in 5–10 drops uniformly distributed onto the water surface (Nanopure, 18.2 M $\Omega$  cm) and left to evaporate and spread evenly over a period of 30 min. When cyclohexane was used, a concentration of 0.1 mg/mL was used. This is less than the critical micelle concentration as determined by dynamic light scattering. During LB deposition, the surface pressure ( $P$ ) was held constant as the submerged substrate was slowly lifted out of the water at a rate of 2 mm/min. The limiting cross-sectional area ( $A_0$ ) was determined at the steep rise in the surface pressure related to the formation of a condensed monolayer.<sup>10</sup>

Highly polished [100] silicon wafers (Semiconductor Processing Co.) were cut into rectangular pieces (2  $\times$  2 cm<sup>2</sup>) and sonicated in Nanopure water for 10 min to remove silicon dust. The wafers were then chemically treated with piranha solution (30% concentrated hydrogen peroxide and 70% concentrated sulfuric acid) for 1 h to strip off any organic and inorganic contaminants clinging to the silicon oxide surface, while at the same time oxidizing/hydroxylating the surface.<sup>23</sup> (**Caution!** Piranha solution is hazardous.) Subsequent rinsing with nanopure water results in a fresh silicon oxide layer with a high concentration of silanol groups. Its thickness was about 1.2 nm, as determined by ellipsometry, and its surface microroughness determined by AFM was below 0.1 nm within the 1  $\times$  1  $\mu\text{m}^2$  surface area.

**Monolayer Characterization.** The effective thickness of the LB monolayers was measured with M-2000 U spectroscopic ellipsometer (J. A. Woolam Co.). UV–vis and fluorescence spectra measurements of the films were performed at room temperature using a UV-1650PC spectrophotometer and a Hitachi F-4500 fluorescence spectrometer. The LB monolayers on the silicon substrates were studied with a Nanoscope IIIa multimode AFM. Scans were performed in light tapping mode in accordance with the usual procedure adapted in our laboratory.<sup>24</sup> An amplitude ratio of  $\geq 0.95$  was employed to avoid monolayer damage (light tapping).<sup>25</sup> The AFM scans were conducted at a 0.5–2 Hz scanning rate for surface areas ranging from 20  $\times$  20  $\mu\text{m}^2$  to 250  $\times$  250 nm<sup>2</sup> and for several randomly selected locations with at least 40 different images collected for each specimen. The domain topography and the surface area coverage were calculated from height histograms using the bearing analysis.<sup>26</sup> The tip radius was measured independently using tethered gold nanoparticles as a standard reference, and only the sharpest tips were selected for high-resolution scanning. The AFM tip radii were between 20 and 35 nm, and the spring constants of these cantilevers were in the range of 40–60 N/m.

(15) Höger, S. *Angew. Chem., Int. Ed.* **2005**, *44*, 3806.

(16) (a) Hsu, H. F.; Chen, H. C.; Kuo, C. H.; Wang, B. C.; Chiu, H. T. *J. Mater. Chem.* **2005**, *15*, 4854. (b) Huang, W. Y.; Gao, W.; Kwei, T. K.; Okamoto, Y. *Macromolecules* **2001**, *34*, 1570.

(17) Harriman, A.; Khatyr, A.; Ziessel, R.; Benniston, A. C. *Angew. Chem., Int. Ed.* **2000**, *39*, 4287.

(18) Tour, J. M.; Rawlett, A. W.; Kozaki, M.; Yao, Y.; Jagessar, R. C.; Dirk, S. M.; Price, D. W.; Reed, M. A.; Zhou, C. W.; Cehn, J.; Wang, W.; Campbell, I. *Chem.–Eur. J.* **2001**, *7*, 5118.

(19) Kushmerick, J. G.; Holt, D. B.; Yang, J. C.; Naciri, J.; Moore, M. H.; Shashidhar, R. *Phys. Rev. Lett.* **2002**, *89*, 086802.

(20) (a) Genson, K. L.; Hoffman, J.; Teng, J.; Zubarev, E. R.; Vaknin, D.; Tsukruk, V. V. *Langmuir* **2004**, *20*, 9044. (b) Peleshanko, S.; Jeong, J.; Gunawidijaja, R.; Tsukruk, V. V. *Macromolecules* **2004**, *37*, 9511.

(21) Kim, J.-K.; Lee, E.; Huang, Z.; Lee, M. *J. Am. Chem. Soc.* **2006**, *128*, 14022.

(22) (a) Larson, K.; Vaknin, D.; Villavicencio, O.; McGrath, D. V.; Tsukruk, V. V. *J. Phys. Chem. B* **2002**, *106*, 7246. (b) Sidorenko, A.; Houphouet-Boigny, C.; Villavicencio, O.; McGrath, D. V.; Tsukruk, V. V. *Thin Solid Films* **2002**, *410*, 147.

(23) Szunerits, S.; Boukherroub, R. *Langmuir* **2006**, *22*, 1660.

(24) (a) Tsukruk, V. V.; Reneker, D. H. *Polymer* **1995**, *36*, 1791. (b) Tsukruk, V. V. *Rubber Chem. Technol.* **1997**, *70*, 430.

(25) Magonov, S. N.; Elings, V.; Whangbo, M. H. *Surf. Sci.* **1997**, *375*, L385.

(26) Magonov, S. N.; Whangbo, M.-H. *Surface Analysis with STM and AFM: Experimental and Theoretical Aspects of Image Analysis*; VCH: New York, 1996.

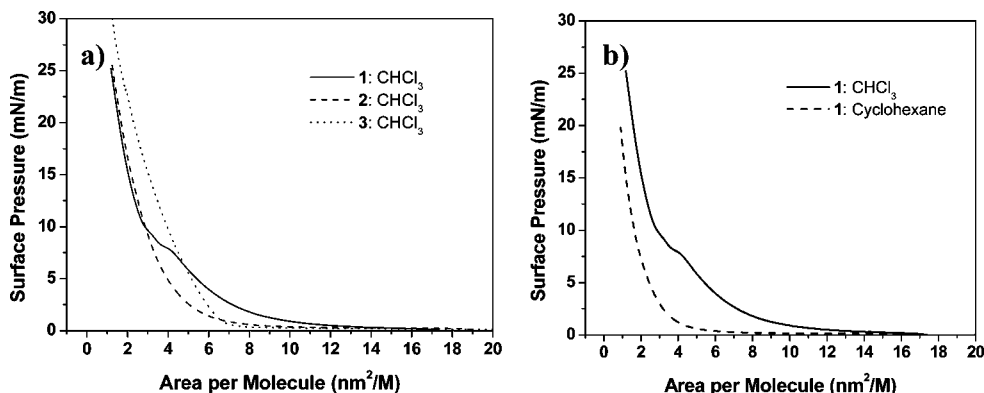


**Figure 2.** (a) Langmuir isotherms for **1**, **2**, and **3**, where  $\text{CHCl}_3$  was used as the spreading solvent. (b) Langmuir isotherms for **1**, where cyclohexane and  $\text{CHCl}_3$  were used as the spreading solvents.

## Results and Discussions

**Behavior at the Air–Water Interface.** The pressure–area isotherms have been collected at several different barrier speeds and waiting times as well as multiple compression–relaxation cycles, all of which generated very similar shapes and parameters (Figure 2). The complete pressure–area isotherm for the molecules by using low-volume solution was technically difficult to obtain within one run because of the limited compression ratio of the LB trough. The collapse surface pressure of **3** using high-volume  $\text{CHCl}_3$  solution is shown at 41 mN/m (Figure S1a). The reversibility of the Langmuir monolayers was examined by repeated cycles of compression and expansion within the low-pressure ( $<5$  mN/m) regime. Minor hysteresis characteristic of the monolayers was observed for **3** (Figure S2a). The surface–area isotherms slightly shift to small areas with increasing cycle number, indicating that the monolayer is relative stable and partially irreversible. Several cycles would lead to the molecules incorporated into monolayers. This is consistent with the AFM images of the films deposited after several cycles (see below), which revealed 3D aggregate formation (Figure 6a). Additionally, the film stability was also checked by measuring the  $\pi$ – $t$  or  $A$ – $t$  isotherms (Figure S2b).<sup>27</sup> The **3** monolayer was compressed to a surface pressure of 2.5 mN/m and held constant at this value for a period of 60 min. The area per molecule decreased to about 4 Å over a 60 min period. This value corresponds to  $<1\%$  of the limiting molecular area of the **3** monolayer. This slight decrease in the surface area is due to the rearrangement of the molecules to reduce the empty spaces in the monolayer or the dissolution of the molecules into water subphase or a partial aggregation of the molecules. Therefore, the film kinetic data suggested the formation of a relatively stable monolayer, and the molecules seldom dissolved into the water subphase.

The isotherms for different compounds (Figure 1) show different shapes. A substantial poly(ethyleneoxide) (PEO) role in the molecular behavior at the air–water interface is evident from the appearance of a shoulder transition for **1**, which possesses the shortest alkyl chain. The observed shoulder indicates the transition of the PEO chains from the pancake conformation flattening on the water surface to a mushroom conformation dissolving into the water subphase. Such behavior is well documented for PEO-containing molecules upon compression.<sup>13,28</sup>

**Table 1.** Characterization and Surface Properties of the Molecules

molecules	molecular length (nm) <sup>a</sup>	$f_{\text{PEO}}^b$	limiting surface area (nm <sup>2</sup> )		pressure (mN/m) in $\text{CHCl}_3$	thickness (nm) in $\text{CHCl}_3$
			in $\text{CHCl}_3$	in cyclohexane		
<b>1</b>	8.3	0.68	3.32	2.43	2	0.51
<b>2</b>	8.8	0.60	3.51	3.51	2	0.48
<b>3</b>	9.3	0.54	4.65	4.65	0.5	0.44
<b>3</b>					2	0.54
<b>3</b>					5	0.65
<b>3</b>					10	1.35

<sup>a</sup> The molecular length was measured by the Corey–Pauling–Koltun (CPK) model. <sup>b</sup>  $f_{\text{PEO}}$  is the volume fraction of PEO.

In contrast, for **2** and **3**, there is a steady increase in the surface pressure up to 25 mN/m upon compression of the monolayers below 2 nm<sup>2</sup>/molecule. Despite the fact that the PEO chain lengths are equal for **2** and **3**, no shoulder transition is observed in the isotherms. This difference may be due to the relatively small PEO content of **2** and **3** as compared to that of **1** (chemical compositions in Table 1).

The limiting cross-sectional surface area per molecule ( $A_0$ ), calculated by the extrapolation of the steep rise in the surface pressure to a zero level, is shown in Table 1. The theoretical surface area occupied by the hydrophobic parts was calculated to be within 3.2–4.6 nm<sup>2</sup> depending upon the alkyl chain length.<sup>29</sup> The values calculated are close to the limiting area measured for all molecules, indicating that the aromatic rod segments adopt a face-on orientation rather than the titled orientation.<sup>9,30</sup> This behavior confirms the critical role of the aromatic parts in the surface behavior of the Langmuir monolayer at high surface pressure.

When another spreading solvent, cyclohexane, was used in place of chloroform, the shoulder on surface isotherms disappeared for **1** (Figure 1b). In this case, the limiting cross-sectional area per molecule decreased to 2.4 nm<sup>2</sup>. This may be due to the fact that **1** could not perfectly dissolve in the hydrophobic solvent of cyclohexane and the PEO chains shrink to some extent. In contrast, for **2** and **3**, no notable changes to their isotherms were observed (Figure S1). This is caused by the shrinkage of the highest-content PEO chains of **1** being more visible than for **2** and **3** in cyclohexane. For **2** and **3**, however, the influence of the

(27) Ji, X.; Wang, C.; Xu, J.; Zheng, J.; Gattas-Asfura, K. M.; Leblanc, R. M. *Langmuir* **2005**, *21*, 5377.

(28) Bijsterbosch, H. D.; de Haan, V. O.; de Graaf, A. W.; Mellma, M.; Leemakers, F. A. M.; Cohen Stuart, M. A.; van Well, A. A. *Langmuir* **1995**, *11*, 4467.

(29) The molecular length was measured by the Corey–Pauling–Koltun (CPK) model, as shown in Figure 1 (scale bar), so the surface area occupied by hydrophobic parts can be calculated.

(30) (a) Kim, J.; Swager, T. M. *Nature* **2001**, *411*, 1030. (b) Kim, J.; Levitsky, I. A.; McQuade, D. T.; Swager, T. M. *J. Am. Chem. Soc.* **2002**, *124*, 7710.

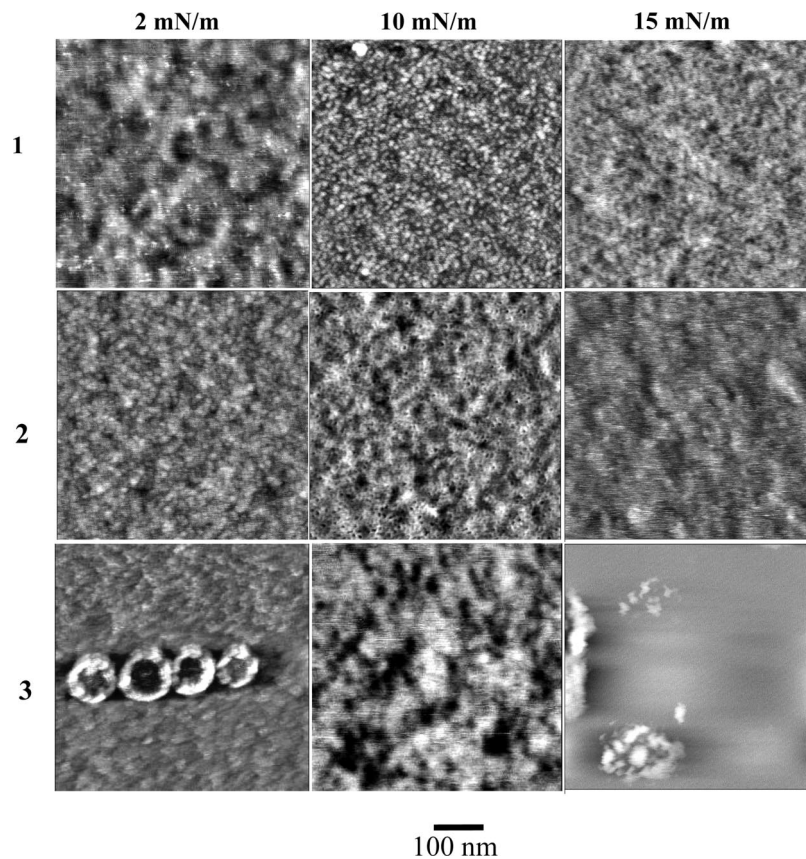


**Figure 3.** High-magnification AFM topography of LB monolayers obtained from chloroform spreading solvent. The  $z$  range is 5 nm.

selective solvent is seen from the change in aggregation behavior (discussed below). Nevertheless, similar pancake-to-mushroom transitions are expected in all cases when a universal solvent, chloroform, was used.<sup>9c</sup>

#### Morphology and Aggregation at the Solid–Air Interface.

The surface morphology of LB monolayers is generally smooth, with a surface microroughness about 0.2 nm (calculated within  $1 \times 1 \mu\text{m}^2$ ), as expected for low-molecular-weight rod–coil molecules as well as for many flexible macromolecular materials.<sup>31</sup> In all cases, AFM images show the full area coverage of the Langmuir–Blodgett monolayer film and a high film-transfer ratio (above 0.9). This indicates that the morphology of the formed monolayer at the air–water interface is preserved upon transfer.<sup>32,33</sup> The effective thickness of the LB monolayer deposited at a surface pressure of 2 mN/m is very small, within 0.4–0.5 nm (Table 1). Such low values confirm the flat, face-on arrangement of the rigid cores tethered by the spread PEO chains at the air–water interface without any microphase separation of dissimilar fragments. At a high surface pressure of 15 mN/m, the molecular area was reduced to 2.06 nm<sup>2</sup> for **1**, 2.22 nm<sup>2</sup> for **2**, and 3.11 nm<sup>2</sup> for **3**, respectively. The values are all smaller than the limiting molecular area of the three molecules (Table 1). In this state, the PEO chains would dissolve in water, and the sharp increase in the surface pressure mainly shows the effect of the rigid hydrophobic segments. Films deposited at this surface pressure revealed 3D aggregate formation. The domain dimensions are several hundred nanometers in width and 10–20 nm

in height (Figure S3). From the corresponding pressure–area isotherms, although no monolayer collapse signal was observed, the AFM images revealed 3D aggregate formation. The local instability of the molecules at the air–water interface that led to the formation of the 3D aggregates may arise from monolayer defects such as dislocations in the plane<sup>34</sup> or molecular tilt.<sup>35</sup> Such defects are introduced when the molecules are spread at the air–water interface and resulted in the protrusion of the molecules into the third dimension. Upon compression, the  $\pi$ – $\pi$  stacking of the aromatic segments and the protrusion of the molecule could act as nucleation points for further aggregate formation.

High-resolution AFM images revealed the shape of the fine molecular aggregates as shown in Figure 3. They were poorly seen for **1** at a low surface pressure of 2 mN/m but became denser and clearly visible upon compression. The sizes of the dots are very uniform with a diameter of 15 nm (while taking into account the tip-dilation effect<sup>36</sup>). This suggests that they are composed of only a few molecules. These dots are formed as the PEO chains were submerged into the water with increasing surface pressure.<sup>9,20</sup> When deposited onto a substrate, PEO chains adsorb onto the hydrophilic surface underneath the hydrophobic backbone and alkyl tails, which translates into increased thickness. At a high surface pressure of 15 mN/m, the dots aggregated further. The surface morphology of LB monolayers for **2**, which is similar to that for **1**, revealed the dot formation at low surface pressure and aggregation at high surface pressure.

(31) (a) Peleshanko, S.; Gunawidjaja, R.; Petrash, S.; Tsukruk, V. V. *Macromolecules* **2006**, *39*, 4756. (b) Peleshanko, S.; erson, K. D.; Goodman, M.; Determan, M. D.; Mallapragada, S. K.; Tsukruk, V. V. *Langmuir* **2007**, *23*, 25.

(32) Genson, K. L.; Vaknin, D.; Villacencio, O.; McGrath, D. V.; Tsukruk, V. V. *J. Phys. Chem. B* **2002**, *106*, 11277.

(33) Riegler, H.; Spratte, K. *Thin Solid Films* **1992**, *210*, 9.

(34) Ybert, C.; Lu, W.; Möller, G.; Knobler, C. M. *J. Phys. Chem. B* **2002**, *106*, 2004.

(35) Saint-Jalmes, A.; Gallet, F. *Eur. Phys. J. B* **1998**, *2*, 489.

(36) Samorí, P.; Francke, V.; Mangel, T.; Müllen, K.; Rabe, J. P. *Opt. Mater.* **1998**, *9*, 390.

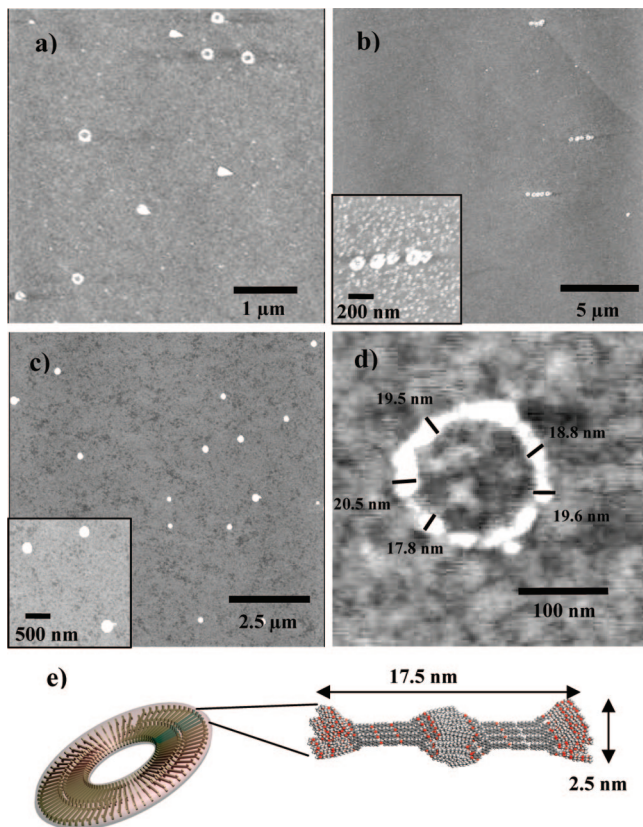


**Figure 4.** AFM topography of **3** at various surface pressures: (a)  $P = 0.5$  mN/m, (b)  $P = 5$  mN/m, (c)  $P = 10$  mN/m, and (d) high-magnification image of the toroid structure at  $P = 0.5$  mN/m. (e) A 2D schematic representation.

It is very interesting that **3** formed a toroid surface structure at a low surface pressure of 2 mN/m (Figure 3). Upon compression, the monolayer became denser, and toroid structures collapsed (Figure 3). The  $\pi$ - $\pi$  stacking of the aromatic segments and the hydrophobic interaction of the alkyl chain would lead to large 3D aggregates as revealed by large scan area AFM images (Figure S3).

**Formation and Stability of Toroid Aggregates.** To investigate the toroid aggregates' formation and stability further, monolayer deposition of **3** at various surface pressures was performed as shown in Figure 4. Individual toroid aggregates were seen even at extremely low surface pressure, below 0.5 mN/m. The effective thickness measured by ellipsometry at this surface pressure (for a molecular area of  $6.11$  nm<sup>2</sup>) was close to the diameter of the molecular chain,  $0.44$  nm (Table 1).

Further increases in the surface pressure up to 5 mN/m (where the molecular area is below the limiting cross-sectional area of  $4.65$  nm<sup>2</sup>) resulted in a slight increase in the monolayer thickness, which reaches  $0.65$  nm. AFM images revealed that at this surface pressure the toroids formed clusters that were unidirectionally aligned along the deposition direction, suggesting that microscopic ordering is controlled by the capillary forces in the course of LB deposition. Next to toroid aggregates, mixed spherical aggregates are occasionally seen (Figure 4b, inset). The toroid aggregates maintained their distinctive donutlike shapes but eventually collapsed into large planar aggregates with an irregular shape at  $P = 10$  mN/m (Figure 4c). The diameter of the aggregates reaches several hundred nanometers. The effective thickness of the film at this molecular area reaches  $1.35$  nm. The 2-fold increase in film thickness is attributable to 3D aggregate formation upon compression. Eisenberg et al. described these large surface

aggregates as large compound micelles.<sup>12a,d,e</sup> In a selective solvent, an amphiphilic block copolymer can self-assemble into large spherical aggregates that can reach several hundred nanometers in diameter. The inner structure of each large compound micelle is filled with bulk reverse 3D micelles<sup>37</sup> whereas in a Langmuir monolayer or LB film the micelle aggregates exist in a 2D scheme (i.e., 2D surface micelle<sup>38</sup>). For an amphiphilic block copolymer, the large compound micelles in LB films correspond to a planar structure, being 2D analogues.<sup>12d</sup> In our case, the large planar aggregates are more irregular and rough compared to surface micelles formed from an amphiphilic block copolymer. This may be due to the incompressible rigid rod segments of the molecules used.

A toroid at high magnification is shown in Figure 4d. The average cross-sectional diameter is about 17 nm as collected from different toroids and different parts of the individual toroid considering the tip dilation.<sup>39</sup> Comparison with the estimated length of a fully extended molecular unit of about 9.3 nm suggests that toroid aggregates are 2D surface micelles composed of an interdigitated bilayer packing of the molecules (Figure 4e). For an evaluation of the lateral size, we should normally consider the horizontal broadening effect due to the shape of the tip, but this is not necessary for the vertical distance.<sup>40</sup> The height of the toroid aggregates estimated from AFM cross-sections is about 2.4 nm. This is consistent with one molecule adopting an edge-on conformation as shown in Figure 4e. It is also worth noting that to some extent short alkyl chains exhibit some compatibility with water.<sup>41</sup>

To further support the orientation of aromatic segments of toroid modeling proposed in Figure 4e, UV-vis and fluorescence spectra were recorded (Figure 5). The absorptions of the LB film deposited at low and high surface pressures exhibit a broadened band centered at 284 nm and a sharp band at 280 nm, respectively, resulting from the conjugated rod block. The fluorescence spectra of the film deposited at low surface pressure show a strong emission maximum at 389 nm, but this maximum is blue shifted to 377 nm for the film deposited at high surface pressure. These results could be attributed to the slightly different intermolecular interactions between adjacent conjugated rods of the film at high and low surface pressures,<sup>42</sup> which consist of large planar micelles at high surface pressure and toroid aggregates with an edge-on conformation at low surface pressure.

It is worth noting that at low surface pressure (e.g., 0.5 mN/m) the monolayer is a mixture of both face-on- and edge-on-oriented molecules (i.e., the toroids adopt an edge-on orientation as implied from AFM height measurement whereas the surrounding molecules that form a smooth monolayer adopt a face-on orientation as confirmed by ellipsometry thickness measurements). Because there are only a few toroids per unit area, the majority of the molecules can be said to adopt the face-on orientation, and hence the area per molecule indicates an average value that is closer to the face-on orientation of the molecules as implied by the limiting molecular area.

(37) Zhang, L.; Eisenberg, A. *Science* **1995**, *268*, 1728. (b) Zhang, L.; Eisenberg, A. *J. Am. Chem. Soc.* **1996**, *118*, 3168.

(38) (a) Cox, J. K.; Eisenberg, A.; Lennox, R. B. *Curr. Opin. Colloid Interface Sci.* **1999**, *4*, 52. (b) Maaloum, M.; Muller, P.; Krafft, M. P. *Angew. Chem., Int. Ed.* **2002**, *41*, 4331.

(39) Ornatska, M.; Peleshanko, S.; Genson, K. L.; Rybak, B.; Bergman, K. N.; Tsukruk, V. V. *J. Am. Chem. Soc.* **2004**, *126*, 9675.

(40) Odin, C.; J. Aim, P.; El Kaakour, Z.; Bouhacina, T. *Surf. Sci.* **1994**, *317*, 321.

(41) McAuliffe, C. *Science* **1969**, *163*, 478.

(42) (a) McQuade, D. T.; Kim, J.; Swager, T. M. *J. Am. Chem. Soc.* **2000**, *122*, 5885. (b) Lee, M.; Jeong, Y.-S.; Cho, B.-K.; Oh, N.-K.; Zin, W.-C. *Chem.-Eur. J.* **2002**, *8*, 876.

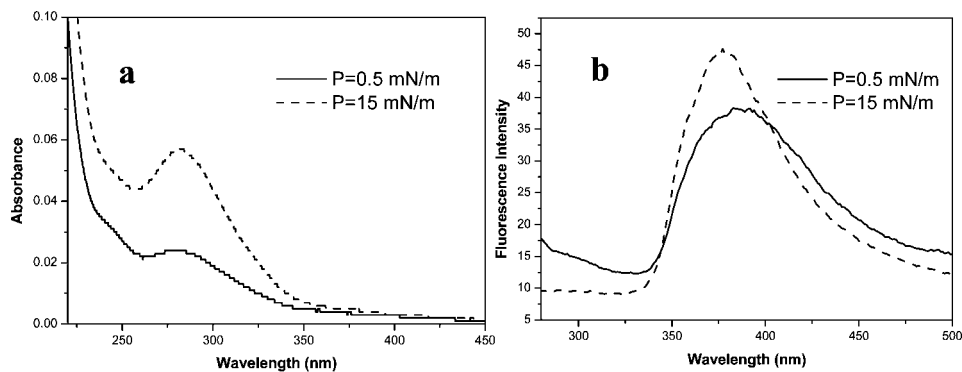


**Figure 5.** (a) UV-vis and (b) fluorescence spectra of 15-layer LB films of **3** deposited on quartz using the  $\text{CHCl}_3$  spreading solvent.

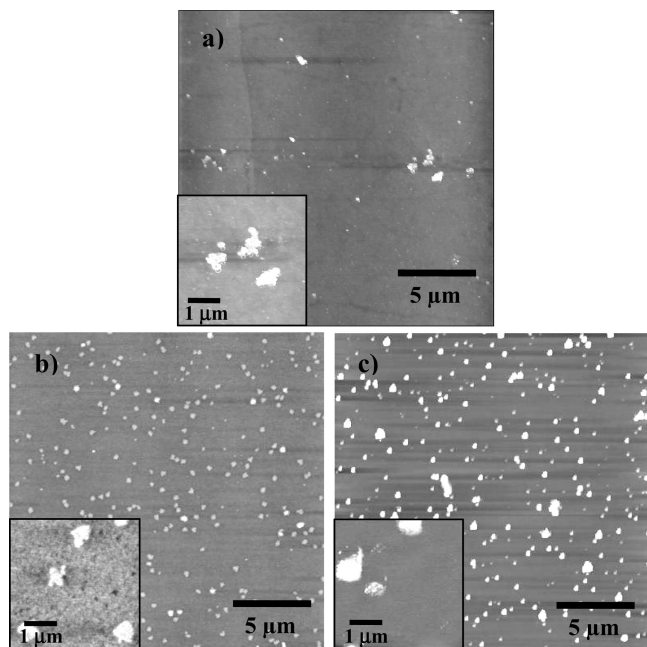


**Figure 6.** AFM topography of (a) cyclic-pressure-induced aggregation for **3** at a modest pressure of 2.5 mN/m and (b) concentration- and (c) surface-pressure-induced aggregation for **3**, both at an equivalent area per molecule at  $P = 20$  mN/m.

In our previous work,<sup>21</sup> the toroid aggregates have been observed to be formed by **2** and maintained a 3D shape in solution. However, at the air-water interface the toroid aggregates are 2D and are formed by **3** with longer hydrophobic tails, indicating that a larger asymmetry of the molecular shape and a higher amphiphilicity are required to sustain toroid aggregation within the monolayer state. The stability of the toroid aggregates was tested by subjecting them to modest cyclic-pressure variation at  $P = 2.5$  mN/m. It was found that the toroid aggregation was relatively stable but collapsed upon compression-expansion cycles with molecules reorganizing into irregularly shaped aggregates (Figure 6a).

Alternative to increasing the surface pressure to induce the further formation of toroid aggregates, a high-concentration solution (0.5 mg/mL in  $\text{CHCl}_3$ ) was spread onto the air-water interface to give an equivalent area per molecule at a surface pressure of  $P = 20$  mN/m (Figure 6b). Whereas a similar density of nontoroidally shaped aggregates is achieved for both concentration- and surface-pressure-induced aggregation, the aggregates look more defined for the concentration-induced aggregation; compare parts b and c of Figure 6 for concentration-versus surface-pressure-induced aggregation.

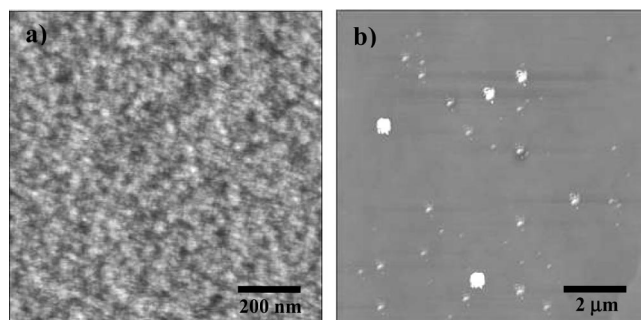


**Figure 7.** AFM topography of LB-deposited **3** at surface pressures of (a) 2 and (b) 10 mN/m using cyclohexane as the spreading solvent.

Furthermore, the influence of the spreading solvent on toroid formation was examined. The chloroform spreading solvent was replaced with hydrophobic solvent cyclohexane. For **1** and **2**, the surface morphologies were not affected when the spreading solvent was changed (Figure S4). In sharp contrast, **3** formed no toroid structures. Instead, uniform monolayer films were formed at low surface pressure, and large planar aggregates were obtained upon compression (Figure 7).

Different mechanisms for the formation of the surface aggregates have been proposed, such as the transfer of micelles in the spreading solution to the surface,<sup>13b</sup> compression-induced surface aggregation formed at a critical micelle concentration driven by compression,<sup>43,44</sup> and a spontaneous surface aggregation process that is neither compression- nor spreading-solvent-dependent.<sup>14</sup> Different mechanisms dominate depending on the molecular weight of each block and the solution concentration. Because dynamic light scattering shows no large aggregates at the present solution concentration, the first mechanism can be excluded for our conditions.<sup>13</sup> The toroid aggregates of **3** are formed even at a surface pressure of 0.5 mN/m and are dependent upon the spreading solvent concentration. This behavior is different from the ring-shaped aggregates formed using a high concentration of solution during solvent evaporation.<sup>45</sup>

Our experimental results suggest that, in the initial stage, presumably upon contact with the water surface, the molecules spontaneously aggregate into 2D spherical aggregates consisting of a hydrophobic core surrounded by hydrophilic dendritic chains with the molecules in an edge-on conformation. Subsequently, the 2D spherical aggregates coalesce into a ringlike structure to reduce the contact area between hydrophobic segments and water

(43) An, S. W.; Su, T. J.; Thomas, R. K.; Baines, F. L.; Billingham, N. C.; Armes, S. P.; Penfold, J. *J. Phys. Chem. B* **1998**, *102*, 387.

(44) Israelachvili, J. *Langmuir* **1994**, *10*, 3774.

(45) Gao, G.; Wang, T.; He, J.; Chen, X.; Yang, Y. *Macromolecules* **2007**, *40*, 2613.

molecules. A higher concentration of molecules at a high surface pressure leads to spontaneous aggregation into large planar aggregates. The formation of toroid aggregates by **3** may be due to the hydrophobic interaction produced from the longest alkyl chain and the unidirectional  $\pi$ - $\pi$  stacking interaction between the aromatic segments confined to a planar monolayer. However, when the hydrophobic solvent, cyclohexane, was used, although the isotherm was almost the same compared with that for the chloroform spreading solvent, the degree of stretching of the PEO chain would slightly decrease.<sup>46</sup> This alleviates the tendency for the hydrophobic segments to move together and aggregate into large planar micelles.<sup>47</sup> In addition, a chloroform/methanol cosolvent mixture (15/85 and 85/15 v/v), which represents a hydrophilic spreading solvent, was used (Figure S5). Little change was seen in the isotherms. AFM measurement of the transferred monolayer did not show the presence of toroid aggregates. In contrast with cyclohexane, a mainly hydrophilic spreading solvent causes the hydrophobic segment to shrink. The shrinking alkyl chain indicates the absence of alkyl-alkyl chain interaction and possibly impedes  $\pi$ - $\pi$  stacking, which are the necessary driving forces for the formation of toroid aggregates. Finally, when the mica substrate was used, a similar toroid structure was obtained for **3** when chloroform was used as the spreading solvent (Figure S6). This indicates that the toroid aggregates were formed at the air-water interface, not during transfer. Direct proof of the spontaneous toroid aggregate may be best observed using in situ

(46) The shrinking of the PEO chain was further proved by using a more hydrophobic spreading solvent (e.g., hexane). The isotherm (Figure S1c in the Supporting Information) was slightly removed to smaller molecular area compared with using chloroform spreading solvent. This indicates that the PEO chain was shrunk to some extent. The AFM images of the film deposited using hexane solvent do not show much difference, only the aggregate formed at relatively low surface pressure compared with using cyclohexane solvent. This further confirmed the critical role of the hydrophobic segments in the formation of toroid structures.

(47) Wen, G.; Chung, B.; Chang, T. *Polymer* **2006**, *47*, 8575.

measurement with Brewster angle microscopy (BAM) because the small toroid dimensions (in the 100 nm range) may not be suited to this technique.

## Conclusions

The formation of unique 3D toroid aggregates reported earlier in solution was closely examined at the solid-air interface. Similar toroid aggregates were found to form spontaneously at the air-water interface but in two dimensions when chloroform was used as the spreading solvent. The combination of AFM analysis, UV-vis and fluorescence spectra, and molecular models shows that these toroid aggregates are composed of interdigitated bilayer packing of the molecules adopting an edge-on orientation at the air-water and air-solid interfaces; they make up only a small majority, such that the surrounding molecules adopt a face-on orientation. The toroidal structures were relatively stable within a range of surface pressures and a certain spreading solution concentration. The formation of toroid aggregates by **3** may be due to the dominating hydrophobic interactions by the longest alkyl chain and  $\pi$ - $\pi$  stacking interactions between the aromatic segments confined to a planar monolayer.

**Acknowledgment.** This work was supported by the National Creative Research Initiative Program. The BK21 program from the Ministry of Education and Human Resources Development and NSF-DMR-0646958 are gratefully acknowledged. We thank Dr. Sergiy Peleshanko for technical assistance with the LB measurements.

**Supporting Information Available:** Langmuir isotherms, large scan area AFM topography, high-magnification AFM topography, and toroid structure. This material is available free of charge via the Internet at <http://pubs.acs.org>.

LA8023106